MEASURED PERFORMANCE OF EVAPORATION DUCT MODELS

L.T. Rogers and R.A. Paulus
Propagation Division

NCCOSC RDTE DIV D883
49170 PROPAGATION PATH
SAN DIEGO CA 92152-7385
fax: (619) 553-1417

ph: (619) 553-1413
email: trogers@nosc.mil

ph: (619) 553-1424
email: paulus@nosc.mil

Abstract

Performance measures are applied to data from the NATO Research Study Group 8 propagation experiment Lorient 1989, to evaluate evaporation duct models. The data set consists of slightly-beyond-line-of-sight propagation data and mid-path meteorological data for over 6000 points in time. Evaporation duct profiles are calculated using three well-known evaporation duct models. Propagation estimates at 3.0 and 10.5 GHz are calculated using those evaporation duct profiles as inputs to a parabolic equation model and are compared to measured propagation. Composite accuracy statistics and accuracy statistics conditioned on relevant parameters are computed. Remote sensing techniques are applied to isolate those periods where the evaporative ducting is the dominant mode of propagation and the same accuracy statistics are re-computed for that subset of the data.

The analysis of the data illustrates the following important points: (1) quantitative performance measures can be applied to the evaluation of refractivity assessment systems, (2) the sampling is uniform over time, as is the operational use of refractivity information, and (3) any conditioning of the data is explicitly noted, rule based, and results are compared to statistics where the conditioning has not been applied.

INTRODUCTION

A recent resurgence of interest in bulk meteorological models of the marine atmospheric surface layer with application to the evaporation duct has prompted are-examination of these models and the meteorological measurements required as inputs. The Integrated Refractive Effects Prediction System (IREPS) was introduced aboard US Navy ships in 1978 utilizing a surface layer model formulated in terms of potential refractivity [*Jeske*, 1971, 1973]. Jeske's algorithm has a simple determination of stability and assumes the empirical universal stability functions follow the KEYPS formula. An empirical modification to this model was subsequently applied to spuriously stable atmospheric conditions arising from thermal distortion due to the ship [*Paulus, 1985].* This characterization of the evaporation duct has been *used* in radiowave propagation assessment for the past decade

Within the meteorological community, a widely accepted bulk formulation for the marine atmospheric surface layer is that of *Liu, Katsaros, and Businger [1979].* The LKB model is more physically rigorous than the Jeske model with an iterative approach to the determination of stability and uses empirical stability functions for temperature and moisture proportional to the square of the KEYPS formula.

These surface layer models require bulk measurements of air temperature, relative humidity, and wind speed at known heights along with a measurement of sea surface temperature. *Blanc [1987]* found that bulk methods yield a very crude estimate of the true stability influence and questioned how much is really gained by using a stability dependent. scheme. Previous propagation studies have found that, for common departures from neutrality, the neutral surface layer refractivity profile is representative of the actual propagation conditions *[Anderson, 1990]. An* analysis of a radio-meteorological data set collected in the Aegean Sea found no statistically significant stability effects in comparing propagation predictions to measured signals [*Paulus*, 1994]. The results of these latter two studies could be argued to represent only open ocean conditions and not be applicable to coastal regions where onshore/offshore winds and strong horizontal gradients in meteorological and oceanographic parameters may significantly impact stability of the surface layer.

This paper provides a brief overview of three bulk meteorological formulations for refractivity in the

surface layer and analyzes the Lorient 1989 radiometeorlogical data set, taken in a coastal environment, using these three formulations as the refractive input to a propagation model.

EVAPORATION DUCT MODELS

A general expression for the gradient of a conservative scalar, S, in the atmospheric surface layer is [*Panofsky and Dutton, 1984]*

$$\frac{\partial S}{\partial z} = \frac{s.}{\kappa z}\varphi_s\left(\frac{z}{L}\right) \quad (1)$$

where z is altitude, S. is the scaling parameter for the scalar, κ is von Karman's constant, L is the Monin-Obukhov length, and φ_S is an empirical stability function for the scalar. Eqn (1) can be integrated from a lower limit of $z=z_0$ to become:

$$S(z) - S_0 = \frac{S_*}{\kappa}\left[\ln\frac{z}{z_0} - \psi_S\left(\frac{z}{L}\right)\right] \quad (2)$$

where zo is the roughness length for the scalar, So is the value of the scalar at altitude z_0, and ψ_S is the integral of the φ_S stability function. S_0, S., z_0, and L are determined from bulk meteorological data at two levels in the surface layer.

Jeske/Paulus. *Jeske's* [1971, 1973] approach was to use potential refractivity, N_p, as the conservative scalar such that eqn (1) becomes

$$\frac{\partial N_p}{\partial z} = \frac{N_{p*}}{\kappa z}\varphi\left(\frac{z}{L}\right) \quad (3)$$

Jeske further determined a characteristic height called the evaporation duct height, δ, the height at which $\partial N_p/\partial z = -0.13$ m^{-1}, the gradient of potential refractivity at which trapping just occurs. Substituting these into eqn (3) yields:

$$-0.13 = \frac{N_{p*}}{\kappa\delta}\varphi\left(\frac{\delta}{L}\right) \quad (4)$$

From eqn (2), in terms of potential refractivity, N_{p*} can be determined from observations of potential refractivity at heights Z_1 and Z_0:

$$N_{p*} = \kappa\frac{N_p(z_1) - N_p(z_0)}{\ln\left(\frac{z_1}{z_0}\right) - \psi\left(\frac{z_1}{L}\right)} \quad (5)$$

where potential refractivity is calculated from

$$N_p = \frac{77.6P_0}{\theta} + 3.73\times10^5\frac{e_p}{\theta^2} \quad (6)$$

Here, $P.$ is a reference pressure (usually 1000 rob), θ is potential temperature in Kelvins, and e_p is potential vapor pressure in mb. Solving eqn (4) for N_{p*} and substituting into equation (3) yields

$$\frac{\partial N}{\partial z} = -0.13\frac{\delta}{z\varphi\left(\frac{\delta}{L}\right)}\varphi\left(\frac{z}{L}\right) \quad (7)$$

Using the relation between potential refractivity and modified refractivity $\partial N_p/\partial z = \partial M/\partial z - 0.13$ [*Gossard and Strauch, 1983]* in eqn (7) and integrating from $z=z_0$ to z,

$$M(z) = M_0 + 0.13z - 0.13\frac{\delta}{\varphi\left(\frac{\delta}{L}\right)}\left[\ln\frac{z}{z_0} - \psi\left(\frac{z}{L}\right)\right] \quad (8)$$

The stability-dependent functions φ and ψ are defined in *Jeske* [1971, 1973]. This model was modified by an empirical correction for spuriously stable conditions [*Paulus, 1985]*

The concept of evaporation duct height has been extremely useful in parametric propagation studies and in development of evaporation duct climatologies. Note in eqn (5) that N_{p*} is proportional to the difference between potential refractivity at the reference height and the surface. Most of the time over the ocean, this difference is negative and thus evaporation duct height calculated in eqn (4) will be positive. However, under certain meteorological conditions that cause subrefraction, the difference in potential refractivity between the reference height and the surface will be positive and a negative duct height will be calculated. The physical interpretation of this negative height is that its absolute value is the height where $\partial N_p/\partial z = +0.13$ m^{-1} or in terms of modified refractivity $\partial M/\partial z = +0.26$ m^{-1}. Since subrefraction is conventionally defined as M-gradients exceeding 0.157 m^{-1}, a negative evaporation duct height generates a subrefractive profile. *Jeske* [1973] referred to this situation as an "anti-duct".

LKB. The LKB approach [*Liu et al.,* 1979] uses potential temperature, θ, and specific humidity, Q, as conservative scalars yielding profiles:

$$\theta - \theta_0 = \frac{\theta_*}{\kappa}\left[\ln\frac{z}{z_T} - \psi_T\right]$$
$$Q - Q_0 = \frac{Q_*}{\kappa}\left[\ln\frac{z}{z_Q} - \psi_Q\right] \quad (9)$$

From the profiles of eqn (9), the profile of modified refractivity is calculated:

$$M(z) = \frac{77.6P}{T} + \frac{3.73\times10^5 e}{T^2} + 0.157z \quad (10)$$

and duct height is determined by inspection of the profile for the height at which the minimum M occurs.

Neutral. The neutral evaporation duct model derives from eqns (3)-(8) by assuming neutral stability of the surface layer for which the empirical stability-dependent functions $\varphi \rightarrow 1$ and $\psi \rightarrow 0$ yielding:

$$M(z) = M_0 + 0.13z - 0.13\delta \ln \frac{z}{[z_0)} \qquad (11)$$

Most importantly, since neutral stability is assumed, the measurement of wind speed is no longer required and the air-sea potential temperature difference is nearly zero and the sea surface temperature can be assumed equal to the air temperature to a good approximation. This is tantamount to assuming that the refractive gradient is predominantly dependent upon the gradient of vapor pressure.

RADIO-METEOROLOGICAL DATA SETS

Greek Islands Measurements. The neutral evaporation duct model was applied to a data set collected in the Aegean Sea *[Richter and Hitney, 1988]* using the Radio Physical Optics (RPO) propagation model. These data had previously been analyzed with the LKB and Paulus models [*Paulus*, 1994]. Figure 1 shows the comparison for the 9.624 GHz link (terminals at 4.8 and 4.9 m above msl). Horizontal dashed lines represent free-space (143 dB) and diffraction (191 dB) levels. The neutral duct model is qualitatively comparable to the other two models in predicting signal level. This result might not be surprising considering that stability-dependent effects were not detected in the data in previous analyses. Thus, the investigation was extended to a data set that would be a more strenuous test of the representativeness of neutral profiles.

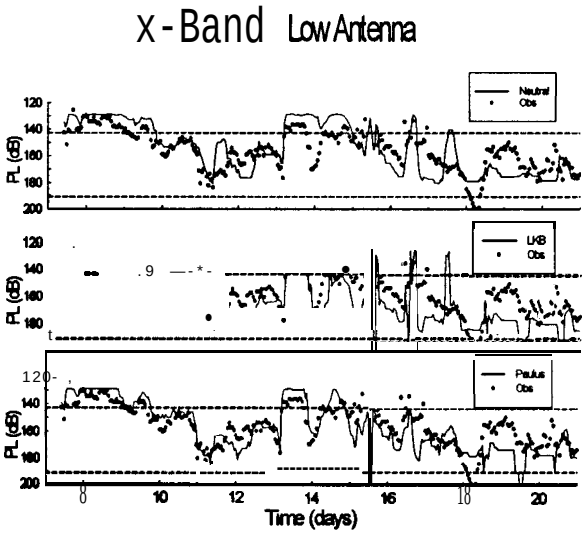

Figure 1. Predicted (solid lines) and observed (dots) propagation loss vs time for neutral, LKB, and Paulus evaporation duct models.

Lorient Radio-Meteorological Measurements. In the fall and winter of 1989, a joint experiment was conducted offshore from the city of Lorient, France on the southwest coast of Brittany [*Claverie and Hurtaud, 1992; Christopher, et al., 1995].* Figure 2 depicts the layout of the Lorient '89 experiment. The experiment was sponsored by NATO Research Study Group 8. The transmitters were located on the Quiberon peninsula and receivers were located at Gavres. The length of the transmission path was 27.7 km. The transmission frequencies, and transmitting and receiving antenna heights referenced to mean-tide level are given in Table 1. This geometry provided for a 4/3 earth horizon range of 25.3 km; however, due to tidal variations of up to 2 m, the link geometry varied from horizon to 1.2 times horizon range. The mid-path buoy shown in Figure 2 was equipped with sensors for wind direction, wind speed (U), relative humidity (RH) and air temperature (T_a). The three sensors were mounted 4.5 meters above the sea surface. The buoy was also equipped with a sea temperature (T,) sensor which was mounted 0.6 m below the sea surface. The tide was monitored at Ile de Groix, approximately 8 km southwest of Gavres.

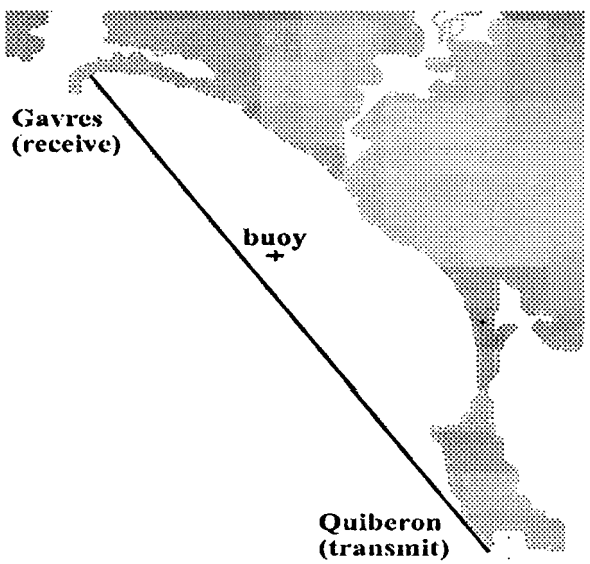

Figure 2. Layout of the NATORSG-8/21 propagation experiment at Lorient, France, 1989, showing the transmitter and receiver sites, the 27.7 km overwater transmission path and location of the mid-path meteorological buoy,

Meteorological and propagation measurements became available on September 23, 1989; 0000Z on that date is considered to be day 0.0 of the experiment. Day 52.0 is the last day that both meteorological and propagation measurements were available. Data were recorded to disk at 10-minute intervals. In the time interval of days 0.0 to 52.0 there were 7488 data points. The data for the tide gage was missing for the interval of days 26.0 to 32.0, reducing the number of available data points to 6624.

Matched data: The following decision rules were used to determine valid data points:

1. Propagation factor measurements are available at both 3.0 and 10.5 GHz.

2. Meteorological inputs for T_a, T_s, RH, U and the tide are available.

3. **All** of the evaporation duct heights calculated using the duct models are below 40 meters. (note: this eliminated a large amount of data, as the LKB model frequently exceeded that threshold with stable input values)

Implementation of the three decision rules reduced the number of data points from 6624 to 6123. The important point regarding the data set of "valid points is that it is the largest set of data containing valid inputs for both the propagation measurements and evaporation duct models.

Evaporative ***ducting*** *subset:* Surface-based ducts can increase signal levels to as much as 10 dB above free space levels, effectively masking the enhancement due to evaporative ducting. For the purposes of evaluating the performance of evaporation duct models, instances where the evaporation duct is not the dominant mode of propagation are "contaminants" in the data. It is desired to determine the subset of the data for which evaporation ducting is the dominant mode of propagation. This is done by using the Bayesian inference procedure described in ***Rogers [1996b].*** The essence of the procedure is that the propagation effects are highly frequency dependent. Using an environmental model including both a surface-based duct and an evaporation duct as the inputs to an EM propagation model, thousands of propagation model runs are performed to determine what combination of propagation measurements are consistent with purely evaporative ducting and which are not. The subset of the valid data where evaporation ducting is believed to be the dominant mode of propagation is referred to as the "evaporation ducting subset" and consists of 5687 points which is **92%** of the valid data points.

The **Bayesian** inference procedure used to **identify** the evaporation ducting subset is a relatively new development. In light of that consideration, overall statistics for both the valid data and evaporation ducting subset are provided also.

Table 1: Link frequencies and transmitter and receiver heights for the **Lorient** '89 experiment.

Frequency (GHz)	**Receiver** ht (m - Avg. Tide)	Transmitter ht. (m - Avg. Tide)
3.0	8.37	10.41
5.6	8.37	10.41
10.5	8.35	10.50
16.0	**8.36**	**10.40**
35.0	**8.23**	**10.27**
94.0	**9.25**	**11.29**

Meteorological ***Representativeness:*** Histograms of the bulk meteorological parameters obtained from the mid-path buoy for the evaporation ducting subset are shown in Figures 3 through 6. Qualitative comparison of the distributions in Figures 3-5 with climatology ***[Gilhousen et al., 1990; U.S. Navy, 1995]*** indicates these are typical of mid-latitude ocean areas. Figure 6, however, is not typical as the mean air-sea temperature difference (ASTD) is normally negative, except in ocean areas influenced by a major ocean front or nearby land mass. Thus, we believe the ASTDS observed during **Lorient** '89 to be typical of many coastal environments rather than open ocean.

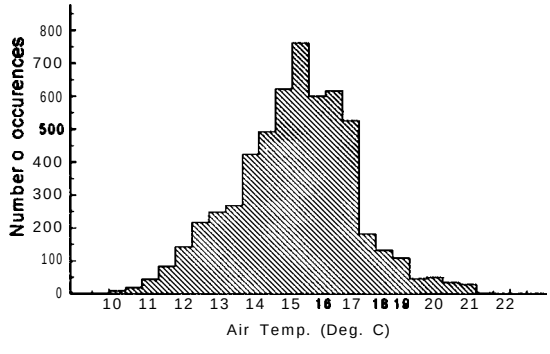

Figure *3.* Air **temperature** histogram,

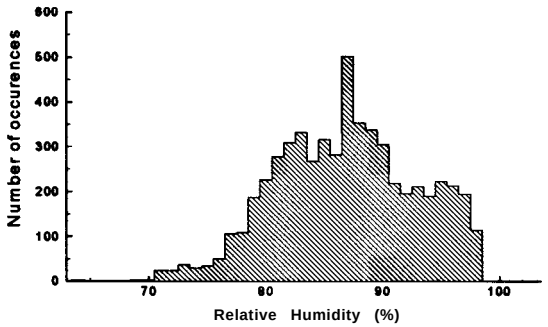

Figure 4. **Relative humidity histogram.**

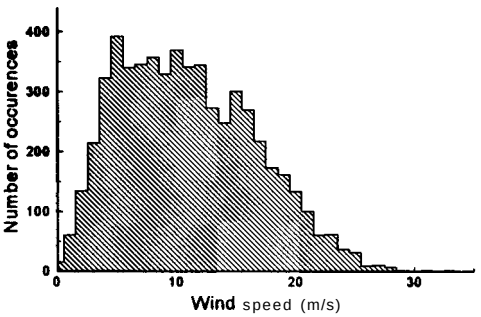

Figure 5. Wind speed histogram

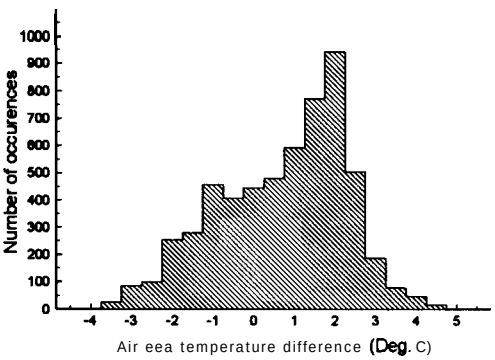

Figure 6. Air-sea temperature difference histogram.

Time series: Figure 7 illustrates the measured and estimated propagation factors for days 2 through 4 on the 3.0 GHz link. Reference lines for free space and standard propagation are provided. The variations in the standard propagation are due to the tide changing the height of the land-mounted transmitters with respect to the sea surface. The heavy solid line is the measured propagation factor. From day 2.0-2.3, 2.9-3.3 and 3.8-4.0 the propagation factor is consistent with evaporation ducting. From day 2.3-2.8 and from day 3.3-3.8, the propagation factor is well above free-space levels. During those intervals, there are deep (10 dB) fades in the measured signal levels. Both of these features are consistent with surface-based ducting. During the surface-based ducting periods, the mismatches between the measured signal levels and those estimated using the three evaporation duct models are quite large. While it appears as though the LKB model does capture the first up-transient, it is also observed that LKB model's subsequent variations are somewhat out of phase with the variations in the measured signals, hence leading to poor real-time estimation performance. For the intervals when the measured signals are consistent with evaporative ducting (days 2.0-2.3, 2.8-3.3, and 3.8-4.0), the performance of the evaporation duct models is quite good, with the LKB appearing to do the best job.

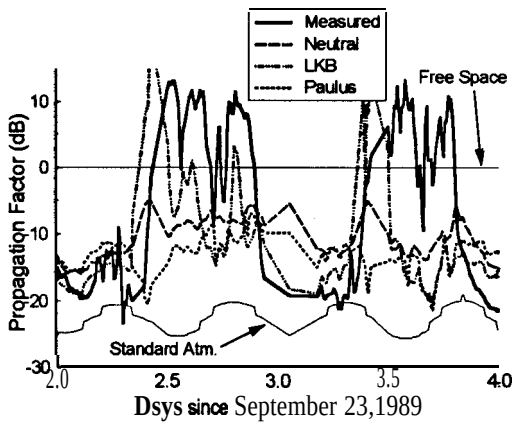

Figure 7. Time series of measured and estimated propagation factor at 3.0 GHz. Reference lines for free space and standard atmosphere are indicated by arrows. The sharp measured signal increases that are seen at days 2.5 and 3.5 are indicative of the onset of surface-based ducting.

In Figure 8, evaporation ducting appears to be the dominant mode of propagation for at least 90% of the time. Overall the performances of the three duct models appear to be comparable except for the transient in the LKB estimates that occurs about day 8.7. which leads the transient in the measured signal levels by 2 to 3 hours. Around day 8.7, the time when

the **measured signal** levels are at a maximum, the LKB estimates are about 20 dB below the measured values.

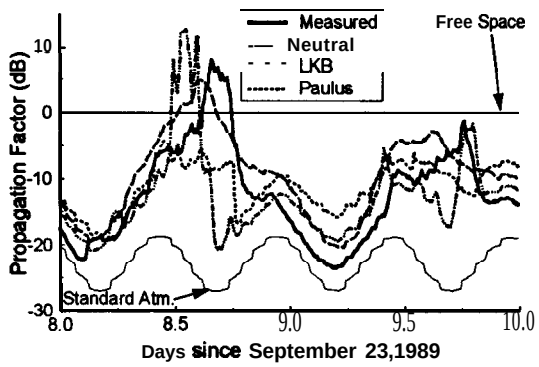

Figure 8. Time series of measured and estimated propagation factor at 3.0 GHz.

STATISTICAL ANALYSIS

Statistics for Measuring Real Time Estimation Performance. Let X and Y **be** propagation estimates and measurements respectively, with means μ_X and μ_Y, **and standard** deviations σ_X **and** σ_Y. **Four** descriptive statistics are commonly used for measuring real-time estimation performance [Rogers, 1996a]:

1. Root mean squared (RMS) error:
$$RMS_{X,Y} = \sqrt{E[(X-Y)^2]} \qquad (12)$$

2. Standard error
$$STD_{X,Y} = \sqrt{E[((X-\mu_X)-(Y-\mu_Y))^2]} \qquad (13)$$

3. Correlation coefficient:
$$\rho_{X,Y} = \frac{E((X-\mu_X)(Y-\mu_Y))}{\sigma_X \sigma_Y} \qquad (14)$$

4. Bias: $b_{X,Y} = \mu_X - \mu_Y$ (15)

If the estimation errors (i.e., the X-Y 's) are normally distributed and are **time-independent,** then any combination of three of the above statistics constitutes a complete description of the error. The primary statistic for evaluating real-time propagation estimation performance is the RMS error. Minimizing the RMS error implies minimizing both the standard error and the bias, and maximizing the correlation. The reverse, however, is not true as is seen here:

$$RMS^2_{X,Y} = \sigma^2_X + \sigma^2_Y - 2\sigma_X \sigma_Y \rho_{X,Y} + b^2_{X,Y} \qquad (16)$$

The square of the RMS error is the sum of the squares of the standard error and the bias:

$$RMS^2_{X,Y} = STD^2_{X,Y} + b^2_{X,Y}. \qquad (17)$$

While the RMS error should be used as the **primary** performance indicator, it should still be used in conjunction with the bias. For example, there might exist two models, both having an RMS error of 7.0. With model "A" the standard error is 7, so the bias is O. With model "B the standard error is O and the bias is 7.0. It is then found that applying smoothing to the model "A" estimates reduces the standard error to 3 dB; consequently, the RMS error of model "A" would be reduced to 3 dB. If the smoothing were then applied to the model "B" data though, it would have no effect. Had only the RMS error been examined, it would have been concluded that the models were essentially identical. If both the RMS error and bias are examined, it would be observed that model "A" appears to be somewhat noisy, but reasonably accurate. Model "B on the other hand appears to have a serious problem as it consistently over-estimates or under-estimates values.

Bias Conditioned on the Air-Sea Temperature Difference. The bias at 3.0 GHz, conditioned on the air-sea temperature difference is shown in Figure 9. Observations include:

1. For ASTD values of less than 0° C, the LKB model performs the best (its bias has the smallest magnitude; it is closest to the O bias) although the performance of the neutral model is only marginally worse.

2. For ASTD values of 0° C and higher, the neutral model performs the **best,** with a bias of about 3 dB. Particularly at very high ASTD values the LKB model performs poorly, with up to a -7 dB bias.

3. It should be noted that the standard atmosphere model shows nearly as much skill at ASTD values of less than 0° C as the models driven by meteorological inputs. The reason is relatively low sensitivity of propagation at 3 GHz to evaporation ducts.

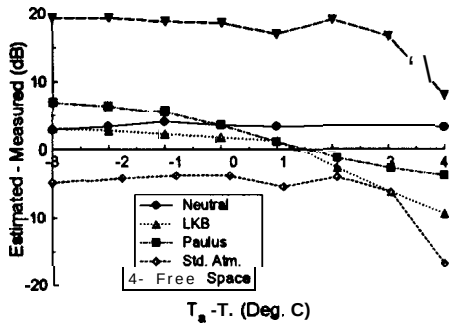

Figure 9. Bias at 3.0 GHz.

Bias at 10.5 GHzisshown in Figure 10. The results are similar except:

1. At ASTD values of greater than 0°C the performance of the Paulus and neutral models is comparable.

2. Standard propagation shows little skill as an estimator of propagation, while the assumption of free space propagation appears quite good for ASTD values less than 2° C. This is because propagation at 10.5 GHz is enhanced for the range of evaporation ducting conditions for this experiment.

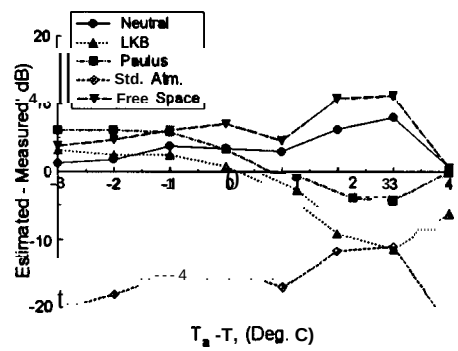

Figure 10. Bias at 10.5 GHz.

RMS Error Conditioned on the Air-Sea Temperature Difference. The RMS error of estimates at 3.0 GHz and 10.5 GHz are shown in figures 11 and 12 respectively. At both frequencies the relative performance of the three duet models are similar: For ASTD values of 0°C or less, the LKB is a dB or so better than the neutral model and 2-4 dB better than the Paulus model. At ASTD values of greater than 1°C, the performance of the neutral and Paulus models is similar, both are substantially better than the LKB.

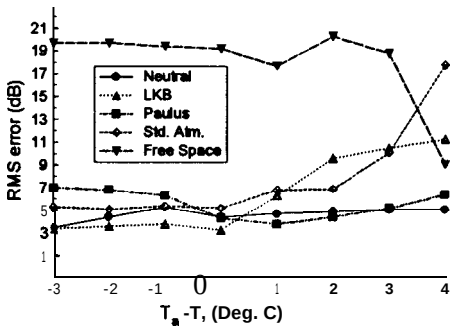

Figure 11. RMS error at 3.0 GHz.

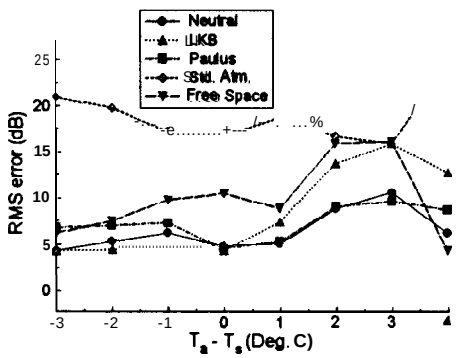

Figure 12. RMS Error at 10.5 GHz.

Overall Performance. The grain of salt that figures 9-12 must be taken with is that some ASTD values occur more often than others. Overall statistics reflect the relative likelihood that a given ASTD value occurs. Tables 2 through 5 provide the complete descriptive statistics for errors of propagation estimates circulated using the neutral (Neu.), LKB, and Paulus (Pau.) method. Errors resulting from the assumption of a standard atmosphere (Std.) or free space (FS) propagation are provided for reference. In each of the tables, [Y is standard deviation of the measured propagation values and $[_x$ is the standard deviation of the propagation estimates calculated using the duct

model listed in the left hand column. Tables 2 and 3 are associated with the evaporation **ducting** subset. Tables 4 and 5 are associated with the set of all valid data points.

Table 2: Overall error statistics at 3.0 GHz for evaporative ducting cases. The total sample size is 5687 points for each value in the table.

	σ_y	σ_x	RMS	STD	ρ	bias
Neu	5.80	5.02	4.79	3.24	.83	3.53
LKB	5.80	8.71	7.30	7.29	.558	-0.29
Pau.	5.80	5.84	5.07	4.79	.662	1.66
std.	5.80	2.50	7.13	5.32	.399	4.75
FS	5.80	0.00	19.09	5.80	-	18.18

Table 3: Overall error statistics at 10.5 GHz for evaporative ducting cases. The total sample size is 5687 points for each value in the table.

	σ_y	σ_x	RMS	STD	ρ	bias
Neu	9.62	6.62	7.05	5.57	.827	4.31
LKB	9.62	14.55	10.04	9.34	.775	-3.69
Pau.	9.62	10.85	7.37	7.37	.747	0.26
Std.	9.62	3.67	17.74	9.64	.185	-14.89
FS	9.62	0.00	12.08	9.62	-	7.31

Table 4: Overall error statistics at 3.0 GHz for both non-evaporative ducting and evaporative ducting cases. The total sample size is 6123 points for each value in the table.

	σ_y	σ_x	RMS	STD	ρ	bias
Neu	7.64	5.27	5.74	5.10	.747	2.64
LKB	7.54	9.44	8.21	8.16	.561	-0.92
Pau.	7.64	5.89	6.48	6.45	.572	0.62
Std.	7.64	2.52	9.56	7.36	.272	-6.09
FS	7.64	0.00	18.49	7.64	-	16.84

Table 5: Overall error statistics at 10.5 GHz for both **non-evaporative** ducting and evaporative ducting cases. The total sample size is 6123 points for each value in the table.

	σ_y	ax	RMS	STD	ρ	bias
Neu	9.67	6.60	6.96	5.71	.819	3.99
LKB	9.67	14.68	10.35	9.68	.758	-3.66
Pau.	9.67	10.72	7.38	7.38	.742	0.09
Std.	9.67	3.67	18.30	9.70	.181	-15.52
FS	9.67	0.00	11.72	9.67	-	6.63

DISCUSSION

The most surprising result is the excellent performance of the neutral model. For unstable conditions, the neutral model performed nearly as well as the best-performing LKB model, and better than the **Paulus** model. For stable conditions, the neutral model outperformed all but the **Paulus** model at 10.5 GHz and performed better than the **Paulus** model at 3.0 GHz.

Another surprising result is the relative performance of the LKB model. For **ASTD>1,** the bias and RMS error both increase as compared to the other two evaporation duct models; for **ASTD<1,** LKB is only slightly better than the neutral model.

ACKNOWLEDGEMENT

The Lorient '89 radio-meteorological data set was provided courtesy of NATO AC 243 Panel 3 RSG-8. The authors performed this analysis under **Office** of Naval Research, ONR-322, finding.

REFERENCES

Anderson, K.D., "94-GHz Propagation in the Evaporation **Duct,"** ***IEEE Trans. Antennas Propagat., 38(5), 746-753, 1990.***

Blanc, T. V., "The Accuracy of Bulk-Method-Determined Flux, Stability, and Sea Surface Roughness," *J. Geophys. Res., 92*(C4), 3867-3876, 1987.

Christopher, F., N. Douchin, Y. Hurtaud, D. Dion, R **Makarushka,** H. Heemskerk, and K. Anderson, "Overview of NATO/AC 243/Panel 3 Activities Concerning Radiowave Propagation in Coastal Environments," ***NATO AGARD CP-567,*** Paper 27, Feb. 1995.

Claverie, J. and Y. Hurtaud, "Propagation Transhorizon en Atmosphere Marine Modelisation et **Nouveaux Resultats** Experimentaux," ***NATO AGARD CP-502***, Paper 4, Feb., 1992.

Gilhousen, D.B., **E.A.** Meindl, **M.J.** Changery, **P.L.** Franks, **M.G.** Burgin, and D.A. McKittrick, ***Climatic Summaries for NDBC Buoys and Stations, 454*** pp., National Weather Service, National Data Buoy Center, NSTL, Miss., Feb. 1990.

Gossard, E.E. and **R.G. Strauch,** ***Radar Observation of Clear Air and Clouds, New*** York: **Elsevier,** 1983.

Jeske, H., "The State of Radar-Range Prediction Over Sea," in Tropospheric Radio Wave Propagation Part II, *NATO AGARD CP-70*, Paper 50, Feb 1971.

Jeske, H., "State and Limits of Prediction Methods of Radar Wave Propagation Conditions Over Sea," in *Modern Topics in Microwave Propagation and Air-Sea Interaction, 131-148,* A. Zancla, cd., Reidel Publishers, 1973.

Liu, W. T., K.B. Katsaros, and J.A. Businger, "Bulk Parameterization of Air-Sea Exchanges of Heat and Water Vapor Including the Molecular Constraints at the Interface, *J. Atmos. Sci, 36, 1722-1735, 1979.*

Panofsky, H.A. and J.A. Dutton, *Atmospheric Turbulence, New* York: Wiley, 1984.

Paulus, R. A., "Practical application of an evaporation duct model," *Radio Sci., 20(4), 887-896, 1985.*

Paulus, RA., "Propagation in the Evaporation Duct: Model Predictions and Comparisons to Data," NRaD TR 1644, NCCOSC RDT&E Division, 1994.

Richter, J.H. and H.V. Hitney, "Antenna Heights for the Optimum Utilization of the Oceanic Evaporation Duct," vols. 1 & 2, NOSC TD1209, Naval Ocean Systems Center, Jan 1988,

Rogers, L. T., "Effects of the variability of atmospheric refractivity on propagation estimates," *IEEE Trans. Antennas and Propagat*, vol. 44, no. 4, pp. 460-465, April, 1996a.

Rogers, L. T., "Remote Sensing of Evaporation Ducts Using SHF Propagation Measurements," in Remote Sensing: A Valuable Source of Information, *NATO AGARD CP-582*, pp. *48.1-48.9,* 1996b.

U.S. Navy, *U.S. Navy Marine Climatic Atlas of the World, Ver 1.1,* CD-ROM, Commander, Naval Meteorology and Oceanography Command, Aug. 1995.